Technical Note

Magnetic field sensor using a polymer-based vibrator

Jiang Wu, Kazuhiko Hasebe, Yosuke Mizuno, Marie Tabaru and Kentaro Nakamura

Laboratory for Future Interdisciplinary Research of Science and Technology, Tokyo Institute of Technology, Yokohama 226-8503, Japan

E-mail: wujiang@sonic.pi.titech.ac.jp

CrossMark

Abstract

In this technical note, a polymer-based magnetic sensor with a high resolution was devised for sensing the high magnetic field. It consisted of a bimorph (vibrator) made of poly (phenylene sulfide) (PPS) and a phosphor-bronze foil glued on the free end of the bimorph. According to Faraday's law of induction, when a magnetic field in the direction perpendicular to the bimorph was applied, the foil cut the magnetic flux, and generated an alternating voltage across the leads at the natural frequency of the bimorph. Because PPS has low mechanical loss, low elastic modulus, and low density, high vibration velocity can be achieved if it is employed as the elastomer of the bimorph. The devised sensor was tested in the magnetic field range of 0.1–570 mT and exhibited a minimum detectable magnetic field of 0.1 mT. At a zero-to-peak driving voltage of 60 V, the sensitivity of the PPS-based magnetic sensor reached $10.5\,V\,T^{-1}$, which was 1.36 times the value of the aluminum-based magnetic sensor with the same principle and dimensions.

Keywords: poly (phenylene sulfide), polymer-based vibrator, bimorph, Faraday's law of induction, magnetic field sensor

(Some figures may appear in colour only in the online journal)

1. Introduction

High magnetic field sensing, or low sensitivity field sensing, is the technique for measuring a magnetic field greater than the geomagnetic field [1, 2]. It has a variety of applications, e.g. magnetic memory readout and high-current measurement [1, 3, 4]. Recently, the magnetic sensor having a wide dynamic range and high resolution has been increasingly in demand for the precise sensing of the high magnetic field. Semiconductor-based magnetic sensors, e.g. the Hall-effect sensors, are widely used owing to their small size and low price [5–9][1], but their sensitivity is limited within a small range [6, 7]. Besides, the

$1/f$ noise restricts their resolution [1, 10]. The newly-invented magnetosensitive materials, e.g. magnetoresistive, magnetostrictive, magnetoelectric, and magnetooptical materials, are effective in magnetic field sensing [11–18]. However, their performance is greatly influenced by the synthesis technology [1, 14, 15], which is under intensive investigation to achieve the practical usage of the magnetosensitive materials.

Magnetic fields can be measured based on electromagnetic principles. To date, a variety of magnetometers with dimensions in the order of several hundred micrometers have been successfully fabricated with the microelectromechanical system (MEMS) technology [17–19]. Most of the MEMS magnetometers operated on the basis of the Lorentz force, and employed the cantilever as the basic structure: when a current flowed along the cantilever, the applied magnetic field

---

[1] Honeywell Hall effect sensing and application: http://sensing.honeywell.com/index.php?ci_id=50371

generated the Lorentz force, which led to a deformation of the cantilever. The deformation was measured from the variation in the capacity formed between the deformed cantilever and the static part. This sensor provided a direct-current (DC) output, and its resolution was restricted by the 1/*f* noise.

To raise the signal-to-noise ratio, a method that provides an alternating-current (AC) signal as the output is employed. According to Faraday's law of induction, an AC voltage is generated on a conductive bar vibrating vertically to a static magnetic field. Our research group has devised several kinds of magnetic field sensors with thin piezoelectric ceramic elements [20]. Longitudinal vibration or extensional vibration was used in these sensors. A part of the electrode plated on the piezoelectric ceramic element was used as the sensing wire, while the rest of the electrode was employed for applying an AC voltage to drive the vibration at the mechanical resonance frequency. In this work, bimorph, which is a cantilever sandwiched by two piezoelectric ceramic plates, was employed as the basic structure of the magnetic field sensor, because it has a relatively simple structure and high vibration velocity compared to the previously tested vibrators. The material of the vibrating body has a great influence on the performance of the sensor. The previously tested vibrator had a piezoelectric-ceramic vibrating body, and its maximum vibration velocity was limited to 300 mm s^{-1} due to the fatigue of the piezoelectric ceramic. Our recent previous research found that poly (phenylene sulfide) (PPS), as a functional polymer, exhibited low attenuation for ultrasound even in high vibration amplitude range [21–23]. Besides, MEMS processing, e.g. etching, sputtering, and ferroelectric-film deposition, has been implemented on the flexible organic substrate [24–26], and it indicates that a micro-sized magnetic field sensor may be made with a PPS elastomer. Currently, silicon is used as the substrate in MEMS magnetometers. Because of the high elastic modulus and the small dimensions, the cantilever provided an extremely low deformation, resulting in low sensitivity of the silicon-based MEMS sensor. If PPS replaces silicon as the substrate, the sensitivity of the magnetic field sensor can be markedly increased.

As a preliminary study of the micro-sized polymer-based magnetic field sensor, we fabricate a PPS-based magnetic field sensor with the dimensions of several dozen millimeters, and test its basic performance. The devised sensor operates on the basis of Faraday's law of induction, which is totally different from the principle of the aforementioned sensors (the Lorentz force), though they have the same basic structure, the cantilever.

2. Materials and methods

Figure 1 shows the schematic and dimensions of the magnetic field sensor, which consisted of an exciting part and sensing part:

(1) Exciting part: the bimorph was composed of an elastomer and two rectangle piezoelectric ceramic elements. The PPS-based elastomer was divided into a rectangular part (45 mm in length, 10 mm in width, and 3 mm in thickness) and

a cylindrical head (10 mm in diameter and 5 mm in length). One end of the rectangular part was fixed. Two piezoelectric ceramic plates (C213, Fuji Ceramics, Fujinomiya, Japan) 10 mm in length, 6 mm in width, and 0.5 mm in thickness, were glued onto the surface of the rectangle part of the elastomer to excite the bending vibration in the direction parallel to the *z*-axis.

(2) Sensing part: at the free end of the bimorph, a phosphor-bronze foil 20 mm in length, 2 mm in width, and 0.1 mm in thickness, was glued along the *x*-axis. When there is a uniform magnetic field along the *y*-axis, an output voltage *u* is induced between the leads:

$$u = Blv, \tag{1}$$

where *B*, *l*, and *v* represent the magnetic flux density, the foil length, and the vibration velocity at the free end, respectively.

In this work, we employed a low-mechanical-loss polymer, PPS, as the elastomer. Its elastic modulus and density are 3.45 GPa and 1350 kg m^{-3}, respectively. The damping coefficient measured in air was 0.002 [21–23]. Because the vibration velocity is inversely proportional to the product of the damping factor and the square root of the elastic modulus and density [27], PPS is a suitable material to obtain a high vibration velocity, which results in high sensitivity of the magnetic sensor.

In this work, we connected the foil and the signal conditioning circuit with a 0.3 mm diameter wire, which was also a candidate as the sensing material. It is easier to glue the foil onto the bimorph than the thin wires, because the foil provides a relatively large surface. Thus, we used the foil as the sensing material in this work. Coils are commonly used in the magnetic field sensors to increase the interlinking [11]. However, the sensitivity cannot be increased unless the coil is partially shielded from the magnetic field due to the working principle of this sensor. In figure 2(a), the voltage, *u*, induced from a single foil (wire) equals the product of the magnetic flux density, *B*, the foil length, *l*, and the vibration velocity, *v*. Figures 2(b) and (c) shows a rectangular spiral coil and a helix coil, respectively. In the spiral coil shown in figure 2(b), if we define that the electric potential at P_1 is 0, the electric potential at P_2 equals Blv. Since P_1P_2 and P_3P_4 have the same vibration velocity, *v*, they yield the voltages of Blv and Bl_1v, respectively. Thus, the electric potential at P_4 decreases to $(Blv - Bl_1v)$, which is in proportion to the length change along the *x*-axis, $(l - l_1)$. Similarly, the electric potential at P_8 is $Bv[(l - l_1) + (l_2 - l_3)]$. The output voltage of the spiral coil equals Blv, the same as the output of the foil in figure 2(a). In the helix coil (figure 2(c)), the induced voltage of P_IP_{II} equals the value of $P_{IV}P_{III}$. As can be observed, the helix yields an output voltage of Blv, which is independent of the number of turns. If some foils are parallelly fixed on the bimorph and connected by the leads shielded from the magnetic field, the sensitivity is increased (figure 2(d)), but the sensing system becomes complicated. The vibration velocity becomes low if the foil and the magnetic shielding component are tightly connected. Thus, the unshielded lead needs to be carefully arranged to decrease its negative effect on the vibration performance.
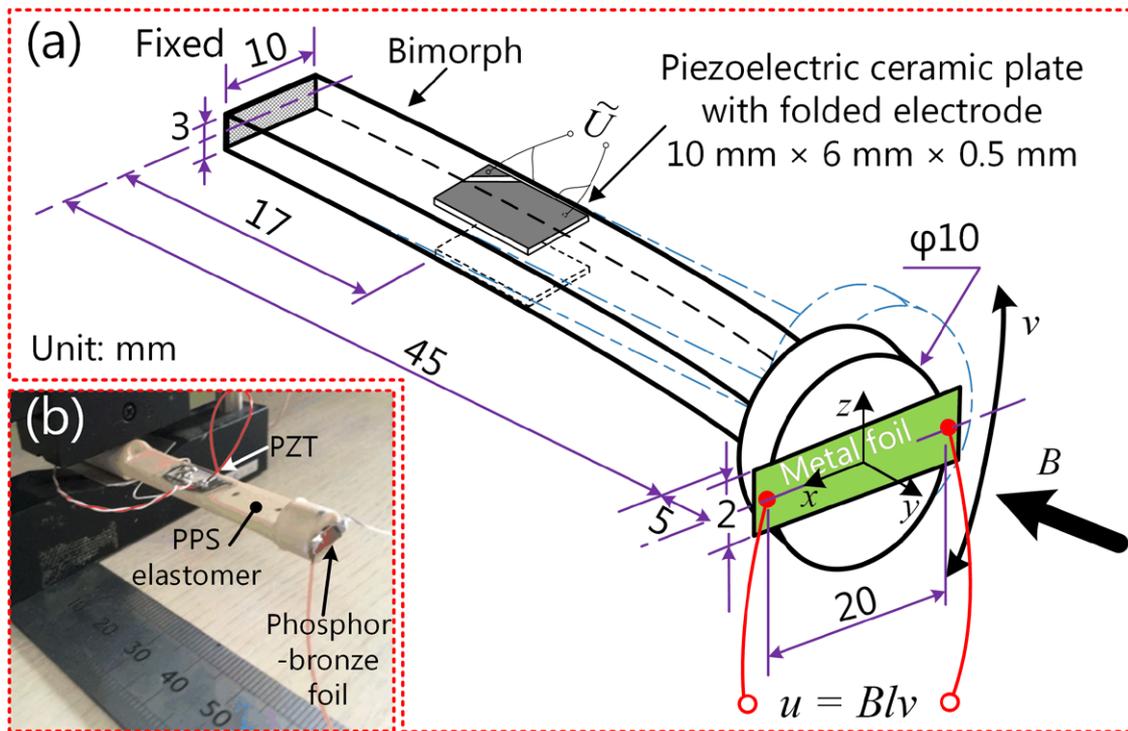
Figure 1. Magnetic field sensor with a PPS-based bimorph: (a) its schematic and dimensions and (b) a picture of the prototype.
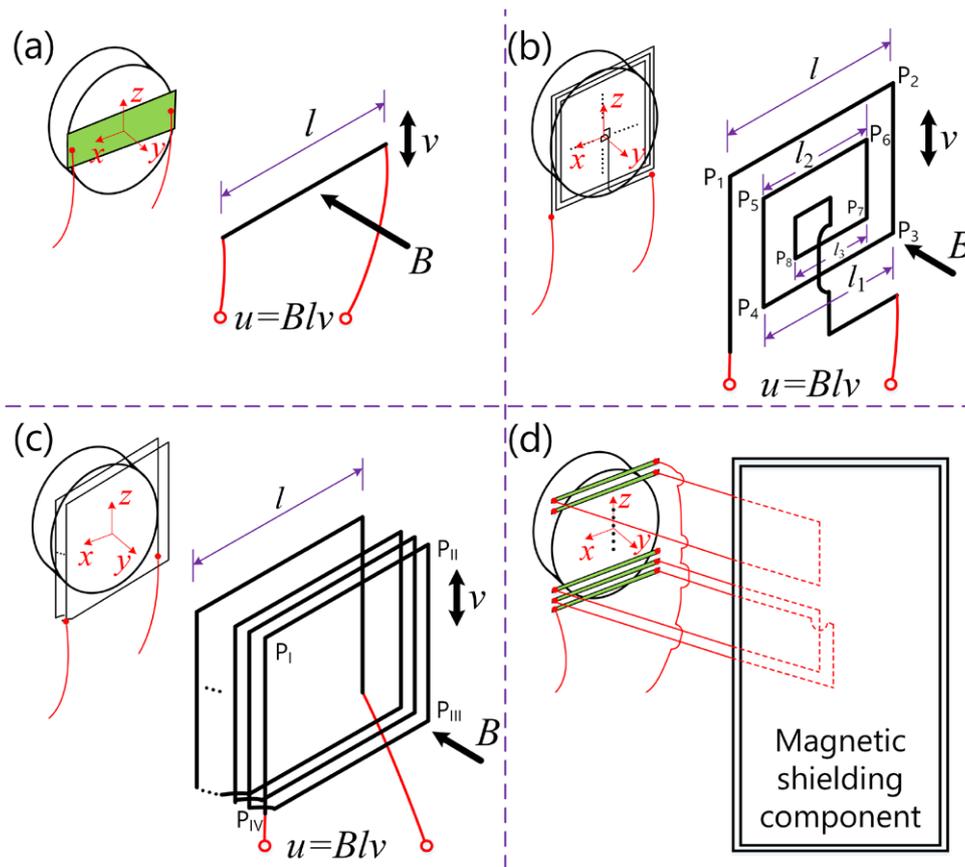

Figure 2. Output voltage induced by (a) a metal plate or wire, (b) a rectangular spiral coil, (c) a rectangular helix coil, and (d) parallel coils connected with magnetic-shielded leads.
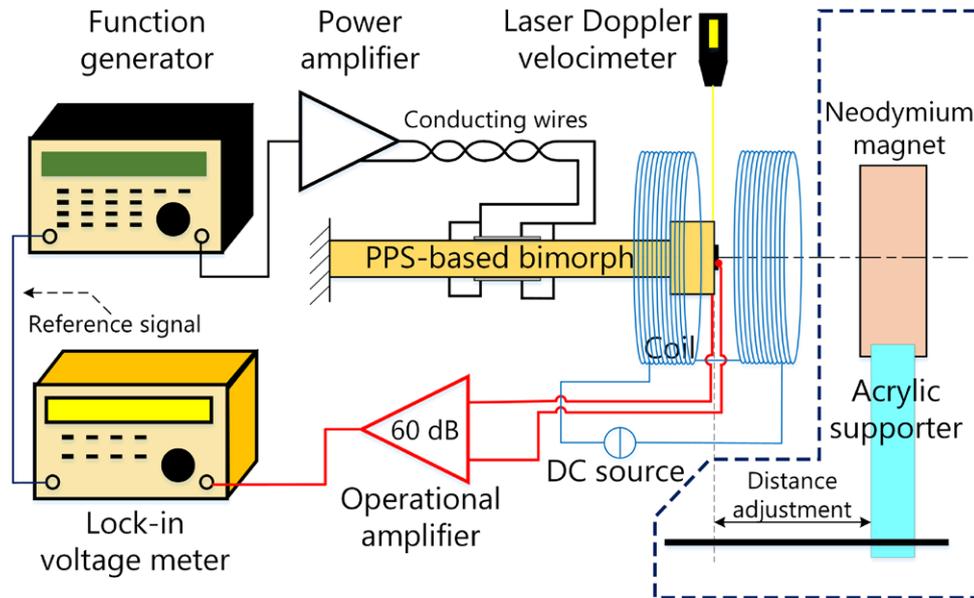
Figure 3. Experimental setup for measuring the magnetic field.

3. Measurement system

Figure 3 shows the experimental setup. The bimorph was driven by a high-intensity AC signal at its natural frequency. The leads were twisted to decrease the mutual inductive coupling between the exciting and sensing circuits. Magnetic fields in the ranges of 0.1–12.5 mT and 12.5–570 mT were generated with a Helmholtz coil and a neodymium magnet, respectively. The Helmholtz coil was electrically connected to a DC power supply. When a DC voltage was applied, a uniform magnetic field of 0.1–12.5 mT was generated inside the coil, and its density was adjusted by changing the current. The Helmholtz coil was composed of two parallel coils 25 mm in length and 60 mm in diameter. The foil was placed at the center of the coil. For calibration, the magnetic flux density at the location of the foil was recorded versus the current using a Hall-effect sensor (A1324, Allegro, Worcester, U.S.). The magnetic field of 12.5–570 mT was generated with a 20 mm diameter 20 mm long neodymium magnet and its density was adjusted by changing the position of the magnet along the y-axis. Using a magnetometer (6010, TOYO, Tokyo, Japan), the magnetic flux density was measured as a function of the z-axis position. Since the magnetic field generated by the neodymium magnet was non-uniform, at a certain position along the y-axis, we measured magnetic flux densities along the x-axis in the range from -10 to 10 mm with an interval of 1 mm. The average value was selected as the magnetic flux density at this position. The leads were electrically connected to the foil edges using the conductive epoxy. The output voltage induced from the foil was conditioned with an instrumentation amplifier (INA118, Texas Instruments, Dallas, U.S.) with a gain of 60 dB. The amplified signal was detected with a lock-in voltage meter (5560, NF Electronic Instruments, Yokohama, Japan). A laser Doppler velocimeter (NLV1232, Polytec, Waldbronn, Germany) was employed to measure the vibration velocity at the free end of the bimorph.

4. Experimental results

First, the optimal frequency was determined. When the zero-to-peak voltage was set to 60 V, the vibration velocity was measured as the driving frequency was swept from 0.01–20 kHz. Figure 4(a) shows that peaks appeared in the vibration velocity versus frequency curve at driving frequencies of 0.31, 1.79, 5.35, 10.12, and 18.05 kHz, which corresponded to the 1st, 2nd, 3rd, 4th, and 5th bending modes, respectively. In particular, at 0.31 kHz, the 1st order bending mode was excited and the vibration velocity reached 360 mm s^{-1}, which was higher than the values at other frequencies. The 5th bending mode yielded a more observable response than the 3rd and 4th bending modes, because the piezoelectric ceramic elements were glued at the place which made it efficient to excite the 5th bending mode. Figure 4(b) shows the voltage dependence of the vibration velocity at approximately 0.31 kHz. The vibration velocity reached 760 mm s^{-1} at 180 V$_{0-p}$. The vibration velocity does not increase linearly with increasing driving voltage, because of the variation in mechanical loss under the high vibration amplitude [21].

Figure 5(a) shows the voltage as a function of the magnetic flux density at the vibration velocities of 10, 50, 100, 200, and 360 mm s^{-1}. Note that the magnetic flux density on the abscissa of figure 5(a) does not include the geomagnetic field. The output voltage increased linearly as the magnetic flux density was varied from 0.1–570 mT, and the minimum detectable difference in the magnetic field was 0.1 mT. The practical range is mainly determined by the input ranges of the preamplifier and the lock-in voltmeter. By adjusting the driving voltage applied to the bimorph, we can easily change the sensitivity to make the output voltage from the lead suitable for the full scale of the preamplifier and the lock-in voltage meter. In figure 4(a), the resolution, defined as the ratio of the minimum detectable change to the dynamic range, reached 0.018%. As mentioned above, this sensor provides
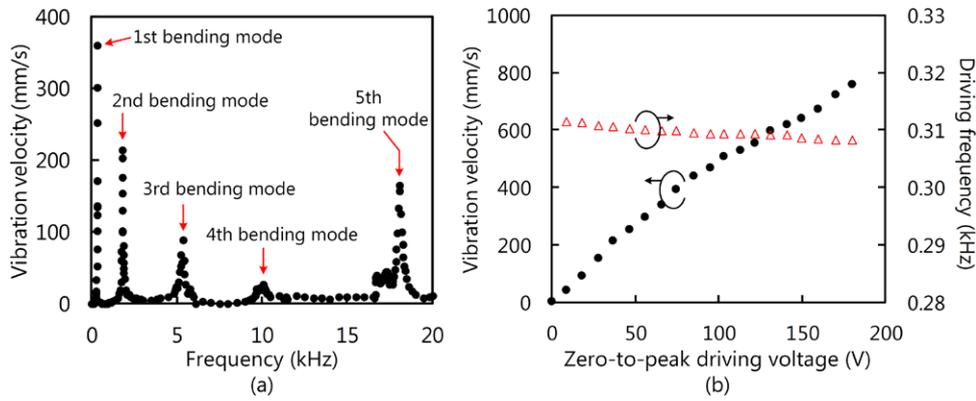
Figure 4. Vibration velocity as functions of (a) frequency at 60 $V_{0\text{-}p}$ and (b) driving voltage at approximately 0.31 kHz.
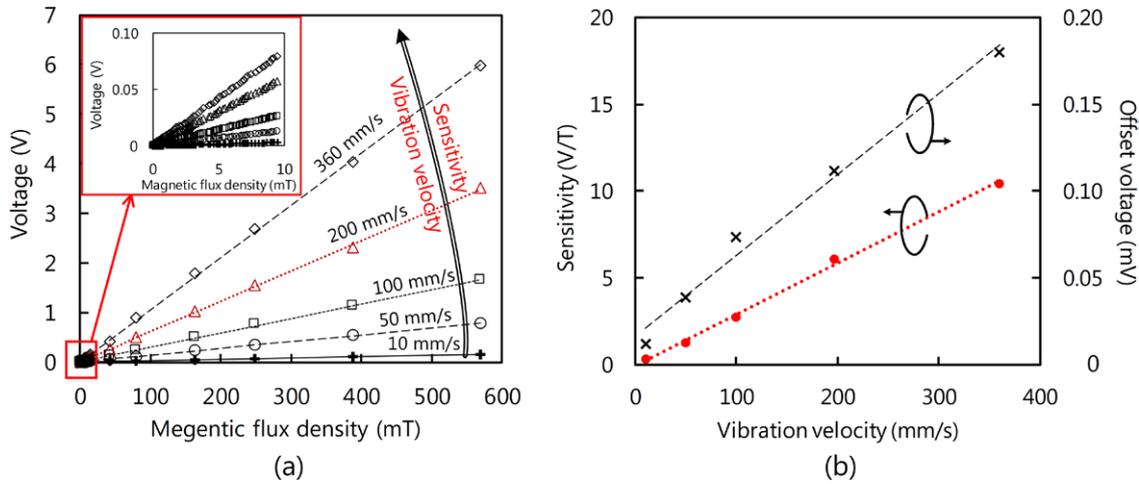

Figure 5. Experimental results: (a) output voltage versus magnetic flux density at vibration velocities of 10, 50, 100, 200, and 360 mm s^{-1}, and (b) sensitivity and offset voltage as a function of vibration velocity.

an AC voltage, which promises a high signal-to-noise ratio by applying a lock-in technique. The output voltage versus magnetic-flux-density curves in figure 5(a) were linearly fitted and the slope of the fitting line was the sensitivity. Figure 5(b) demonstrates how the sensitivity varied with the vibration velocity. The sensitivity was 0.3 V T^{-1} at the vibration velocity of 10 mm s^{-1} and increased to 10.5 V T^{-1} linearly as the vibration velocity increased to 360 mm s^{-1}. Since the maximum vibration velocity reaches 760 mm s^{-1} at 180 $V_{0\text{-}p}$, the maximum sensitivity is expected to be 22 V T^{-1}. The linearity errors at 10, 50, 100, 200, and 360 mm s^{-1} were 1.8%, 2.0%, 1.6%, 1.9%, and 1.6%, respectively. The average value was 1.8%, which was at the same level as the values of commercial magnetic sensors (typically ~1.5%) [5][2].

When the magnetic field was switched off, the magnetic field sensor yielded a harmonic signal, of which the zero-to-peak amplitude was defined as the offset voltage. Figure 5(b) shows that the offset voltage became higher with increasing vibration velocity. It may be attributed to the geomagnetic field and the crosstalk between the exciting and sensing circuit. At 20 $V_{0\text{-}p}$, the signal had the amplitude of 0.078 mV and the phase of 53.5°. After the sensor orientation was reversed, its amplitude and phase were 0.075 mV and −99.1°, respectively.

Clearly, the amplitude had little change, but the phase almost reversed. The geomagnetic field has a dominant effect on the offset, while the crosstalk has a minor contribution.

For comparison, we fabricated an aluminum sensor with the same structure and dimensions as the PPS-based sensor. The foil was glued onto the aluminum bimorph with electric insulating epoxy, which can suppress the electrical interference originating from the power supply. At 0.54 kHz, the aluminum sensor yielded a vibration velocity of 266 mm s^{-1} at 60 $V_{0\text{-}p}$, and had a mechanical quality factor (Q) of 750. The sensitivity was 7.6 V T^{-1}, which was 0.74 times the value of the PPS-based sensor. Although the PPS-based bimorph has a lower Q factor, it exhibited a larger vibration velocity than the aluminum bimorph, because PPS had much lower elastic modulus. In addition, the PPS-based sensor had a weight of 3.2 g, which was 0.55 times the value of the aluminum-based sensor (5.8 g). These results indicate that the high vibration velocity (high sensitivity) and the light weight are achieved by utilizing PPS as the bimorph elastomer.

The glass-transition and melting temperature of PPS are approximately 90 °C and 280 °C, respectively. PPS provides mechanical-property stability before 90 °C [28]. However, in the range of 90 °C–280 °C, its elastic modulus has an observable decrease with increasing temperature, which leads to a variation in the resonance frequency. Thus, in practice the

[2] See footnote 1.

temperature should be <90 °C. PPS products have a typical moisture absorption value of 0.03% at 23 °C for 24h [28]³. The value was relatively low among the commonly-used engineering polymers.

5. Conclusions

On the basis of Faraday's law of induction, a magnetic field sensor with a polymer-based vibrator was devised and its basic performance was tested. The output voltage increased linearly as the magnetic field increased from 0.1–570 mT with a minimum detectable change of 0.1 mT. Compared with the aluminum sensor, the polymer-based sensor exhibited relatively high sensitivity and light weight. A sensitivity of 22 V T^{-1} is expected when the driving voltage applied to the bimorph reaches 180 V$_{0\text{-p}}$. With the simple structure and the inherent performance, this magnetic sensor has the possibility of commercialization if its dimensions are significantly minimized. In the future, the miniaturization of this sensor will be considered based on the MEMS technology. In addition, sophisticated design of the cantilever and the pick-up coil will be carried out.

Acknowledgments

References

[1] Lenz J and Edelstein A S 2006 Magnetic sensors and their applications *IEEE Sens. J.* **6** 631–48

[2] Caruso M J, Bratland T, Smith C H and Schneider R 1998 A new perspective on magnetic field sensing http://www51.honeywell.com/

[3] Popovic R S, Flanagan J A and Besse P A 1996 The future of magnetic sensors *Sensors Actuators* A **56** 39–55

[4] Ripka P 2010 Electric current sensors: a review *Meas. Sci. Technol.* **21** 112001

[5] Ramsden E 2006 *Hall-Effect Sensors: Theory and Applications* (Oxford: Elsevier)

[6] Popovic R S 1989 Hall-effect devices *Sensors Actuators* A **17** 39–52

[7] Milby R, Schreck E and Sonnenfeld R 1998 Measurement of the head-to-disk stiction force in an unmodified hard driving using external Hall-effect sensors *IEEE Trans. Magn.* **34** 1780–82

[8] Mapps D J 1997 Magnetoresistive sensors *Sensors Actuators* A **59** 9–19

[9] Weiss R, Mattheis R and Reiss G 2013 Advanced giant magnetoresistance technology for measurement applications *Meas. Sci. Technol.* **24** 082001

[10] Kotera N, Shigeta J, Oi T, Nakashima M and Sato K 1978 Transverse 1/*f* noise in InSb thin films and the signal-to-noise ratio of related Hall elements *J. Appl. Phys.* **49** 5990–6

[11] Tumanski S 2007 Induction coil sensors—a review *Meas. Sci. Technol.* **18** R31

[12] Ryu J, Carazo A V, Uchino K and Kim H-E 2001 Magnetoelectric properties in piezoelectric and magnetostrictive laminate composite *Japan. J. Appl. Phys.* **40** 4948–51

[13] Du Y, Liu T, Ding Z, Liu K, Feng B and Jiang J 2015 Distributed magnetic field sensor based on magnetostriction using Rayleigh backscattering spectra shift in optical frequency-domain reflectometry *Appl. Phys. Express* **8** 012401

[14] Jin T, Hao L, Cao J, Liu M, Dang H, Wang Y, Wu D, Bai J and Wei F 2014 Electric field control of anisotropy and magnetization switching in CoFe and CoNi thin films for magnetoelectric memory devices *Appl. Phys. Express* **7** 043002

[15] Iyama A, Wakabayashi Y, Hanasaki N and Kimura T 2013 Magnetoelectric effect in FeSb$_2$O$_4$ single crystals *Japan. J. Appl. Phys.* **53** 05FB02

[16] Yanaga M, Shoji Y, Takamura Y, Nakagawa S and Mizumoto T 2015 Compact magnetooptical isolator with cobalt ferrite on silicon photonic circuits *Appl. Phys. Express* **8** 082201

[17] Marauska S, Jahns R, Greve H, Quandt E, Hnochel R and Wagner B 2012 MEMS magnetic field sensor based on magnetoelectric composites *J. Micromech. Microeng.* **22** 065024

[18] Sreenivasulu G, Qu P, Petrov V, Qu H and Srinivasan G 2016 Sensitivity enhancement in magnetic sensors based on ferroelectric-bimorphs and multiferroic composites *Sensors* **16** 262

[19] Li M, Rouf V T, Thompson M J and Horsley D A 2012 Three-axis Lorentz-force magnetic sensor for electronic compass applications *J. Microelectromech. Syst.* **21** 1002–10

[20] Dan K, Nakamura K and Ueha S 2006 A novel magnetic field sensor using piezoelectric vibrations *Proc. 27th Symp. Ultrasonic Electronics (Tsukuba, Japan)* pp 217–8

[21] Wu J, Mizuno Y, Tabaru M and Nakamura K 2016 Measurement of mechanical quality factors of polymers in flexural vibration for high-power ultrasonic application *Ultrasonics* **69** 74–82

[22] Wu J, Mizuno Y, Tabaru M and Nakamura K 2015 Ultrasonic motors with polymer-based vibrators *IEEE Trans. Ultrason. Ferroelectr. Freq. Control* **62** 2169–78

[23] Hill H W and Brady D G 1976 Properties, environmental stability, and molding characteristics of polyphenylene sulfide *Polym. Eng. Sci.* **16** 831–35

[24] Zou H, Zhang Q, Tan H, Wang K, Du R and Fu Q 2006 Clay locked phase morphology in the PPS/PA66/clay blends during compounding in an internal mixer *Polymer* **47** 6–11

[25] Anagreh N, Dorn L and Bilke-Krause C 2008 Low-pressure plasma pretreatment of polyphenylene sulfide (PPS) surfaces for adhesive bonding *Int. J. Adhes. Adhes.* **28** 16–22

[26] Shiraishi T, Kaneko N, Ishikawa M, Kurosawa M K, Uchida H and Funakubo H 2014 Ferroelectric and piezoelectric properties of KNbO$_3$ films deposited on flexible organic substrate by hydrothermal method *Japan. J. Appl. Phys.* **54** 09PA10

[27] Ley B F, Lutz S G and Rehberg C F 1959 *Linear Circuit Analysis* (New York: McGraw-Hill)

[28] Fink J K 2014 *High Performance Polymers* (Oxford: Elsevier)

³ DIC what is PPS: www.dic-global.com/jp/en/products/pps/about.html